



Continuously tunable metasurfaces controlled by single electrode uniform bias-voltage based on nonuniform periodic rectangular graphene arrays

DINGBO CHEN,  JUNBO YANG, *  JIE HUANG,  ZHAOJIAN ZHANG,  WANLIN XIE, XINPENG JIANG, XIN HE, YUNXIN HAN, ZHENFU ZHANG, AND YANG YU 

Center of Material Science, College of Liberal Arts and Sciences, National University of Defense Technology, Changsha 410073, China

*yangjunbo@nudt.edu.cn

Abstract: Metasurfaces, the two-dimensional artificial metamaterials, have attracted intensive attention due to their abnormal ability to manipulate the electromagnetic wave. Although there have been considerable efforts to design and fabricate beam steering devices, continuously tunable devices with a uniform bias-voltage have not been achieved. Finding new ways to realize more convenient and simpler wavefront modulation of light still requires research efforts. In this article, a series of novel reflective metasurfaces are proposed to continuously modulate the wavefront of terahertz light by uniformly adjusting the bias-voltage. By introducing the innovation of nonuniform periodic structures, we realize the gradient distribution of the reflected light phase-changing-rate which is the velocity of phase changing with Fermi energy. Based on strict phase distribution design scheme, a beam scanner and a variable-focus reflective metalens are both demonstrated successfully. Furthermore, dynamic and continuous control of either the beam azimuth of beam scanner or the focal length of metalens can be achieved by uniformly tuning the Fermi energy of graphene. Our work provides a potentially efficient method for the development and simplification of the adjustable wavefront controlling devices.

© 2020 Optical Society of America under the terms of the [OSA Open Access Publishing Agreement](#)

1. Introduction

Metasurfaces are a new kind of two-dimensional artificial materials consisting of properly designed subwavelength structures. In the past decade, metasurfaces have attracted much attention due to its unprecedented properties that are unavailable in nature [1–5]. By introducing the abrupt changes of amplitude, polarization and phase of electromagnetic waves, metasurfaces can modulate the wavefront of light deeply with less non-ignorable energy loss, which is almost impossible to realize by conventional three-dimensional metamaterials [6–9]. Owing to the ultrathin thickness and the design flexibility, metasurface-based optical elements provide great potential in the miniaturization and integration of conventional bulky optical components. Based on the modulation of optical properties of metasurfaces, a multitude of devices with extraordinary properties have been proposed, such as gradient index diffraction grating, beam deflector, surface plasmon couplers, wave plates and holograms [10–17]. In most instances, the optical responses of these devices based on the metallic structures with subwavelength dimensions or the Mie resonances in composite structures consisting of high-index dielectric medium [18–21]. Therefore, the functionalities of most devices demonstrated so far cannot be tuned dynamically after being fabricated, which greatly limits the potential for a variety of applications that need dynamical modulation over the wavefront of electromagnetic waves, such as beam scanner and variable-focusing metalens.

In recent years, the rapid development of viable devices with dynamical responses to the characteristics of incident light has gradually attracted significant interest. Traditional tuning methods are usually limited by small adjustable range or slow response because the tuning mechanism is based on mechanical or thermal [22–25]. By integrating metasurfaces with permittivity adjustable materials, a new method is obtained to actively control the wavefront of electromagnetic waves [26]. Graphene, an acclaimed two-dimensional structure made of mono layered honeycomb arrange of carbon atoms, has been demonstrated to be a potential material for the design and fabrication of infrared and terahertz plasma devices and metasurfaces [27–30]. Especially, the Fermi energy of graphene can be easily adjusted by electrical gating or chemical doping, which is the greatest advantage as a promising material for designing tunable optical devices [31–34]. A variety of graphene-based metasurfaces, with patterned graphene or hybrid graphene-metal composites, have been wildly proved to realize tunable functions such as polarization conversion, antenna emission, perfect absorption and optical transformation [35–38]. Currently, dynamically tunable metasurfaces based on graphene nanostructures have been demonstrated to manipulate wavefront of terahertz light, whose typical functions are beam steering and active-focusing lensing [39–43]. However, in these designs, the realization of continuously tunable beam azimuths or focal spots can only be based on the individual modulation of Fermi energy of each graphene unit. Apparently, it is not practical to individually tune the Fermi energy of each resonator in experimental process. The main implementation difficulty is the complexity in device fabrication and integration, which is caused by the subwavelength dimension of graphene structure [30].

In this paper, we propose a series of novel reflective metasurfaces composed of nonuniform periodic rectangular graphene sheet arrays for wavefront modulation of linearly terahertz waves. By introducing the nonuniform periodic structures, the gradient distribution of the reflected light phase-changing-rate is achieved. As proof-of-concept demonstrations, a beam scanner and a variable-focus reflective metalens using monolayer graphene sheet arrays are designed and numerically verified. More importantly, either the beam azimuth of beam scanner or the focal spot of metalens can be dynamically and continuously controlled by uniformly, rather than separately, modulating the Fermi energy of graphene structures. For beam scanner, its beam azimuth can change from 0° to 35.5° continuously by adjusting the Fermi energy of graphene, when the frequency is fixed at 5 THz. For variable-focus reflective metalens, the range of focal length adjustment from 380 to 660 μm can be achieved at 5 THz. Besides, the scanning function of the scanner and the dynamic focusing function of the metalens are effective in the broadband range. More importantly, the graphene Fermi energy can be easily modulated via adjusting the gate voltage. This work could provide a potential way for the designing of desirable devices that enable us to continuously adjust the wavefront of the terahertz beams and to promote more applications in nanophotonic systems.

2. Structure design and research method

The diagram of the proposed metasurface based on nonuniform periodic rectangular graphene array is shown in Fig. 1(a). To completely eliminate transmission, a gold substrate with optical thickness is placed at the bottom as a perfect reflection layer. A patterned graphene monolayer is transferred to the gold substrate, separated by a dielectric layer (e.g., MgF_2 and SiO_2) with permittivity of 1.90. The dielectric layer thickness (T_m) is fixed at 11.6 μm (see Supplement 1, Note S1 and Fig. S1). An ion-gel layer with a thickness of 0.1 μm is covered over the top of graphene. The ion-gel layer with high capacitance acts as a transparent spacer-layer between the graphene structures and top gold contact [44]. The permittivity of the ion-gel is 1.82 [35]. The composite structure, which is composed of patterned array of rectangular graphene sheets and dielectric/metal substrate, was adopt to manipulate the wavefront of the reflected linear polarized terahertz light. The top view of a group of feature structures consisting of two sections (section I

and section II) is shown in Fig. 1(b). The geometry parameters of graphene unit are shown in Fig. 1(c). In contrast with previous works whose periodicity along x - and y - direction were fixed, our design only fixes the periodicity along y -direction ($P_y = 6 \mu\text{m}$). The value of the periodicity along x -direction P_x is variable. In addition, a new parameter $k = 0.5 \mu\text{m}$ is introduced into our model, which represents the distance between two adjacent graphene sheets. This parameter plays a quite important role in stabilizing the efficiency of the devices. As shown in Fig. 1(c), P_x is the sum of G_x and k .

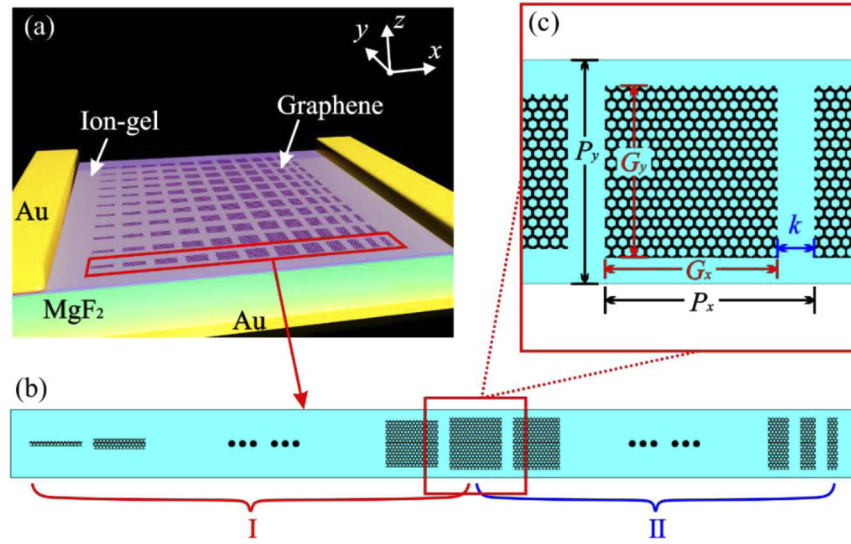


Fig. 1. (a) Schematic representation of the proposed metasurface, which consist of nonuniform periodic rectangular graphene sheet arrays. The thicknesses of the dielectric and ion-gel layer are $11.6 \mu\text{m}$ and $0.1 \mu\text{m}$, respectively. (b) Top view of a group of feature structures including two sections (section I and section II). (c) Sketch of the unit cell containing the rectangular graphene sheet.

In the terahertz region, the surface conductivity of graphene that dominated by the intraband transition can be derived by the semi-classical Drude model [45]:

$$\sigma(\omega) = \frac{e^2 E_f}{\pi \hbar^2} \frac{i}{\omega + i\tau^{-1}} \quad (1)$$

where ω represents the angular frequency, E_f the Fermi energy, τ the electron-phonon relaxation time, e and \hbar are universal constants representing the electron charge and reduced Planck's constant, respectively. The electron-phonon relaxation time can be calculated by $\tau = \mu E_f / v_f^2$, where the carrier mobility is equal to $\mu = 10^4 \text{cm}^2/\text{Vs}$ and the Fermi velocity is equal to $v_f = 10^6 \text{m/s}$. The permittivity of graphene can be calculated from the following equation:

$$\varepsilon_g = 1 + \frac{i\sigma(\omega)}{(\omega \varepsilon_0 t_g)} \quad (2)$$

Here, the ε_0 and t_g are the vacuum permittivity and the thickness of graphene, respectively. In the calculations, we adopt the Finite Element Method (FEM) to calculate the electromagnetic response of the graphene array. To reduce the calculation difficulty and save time, the finite film thickness is replaced by the transition boundary condition, and the conductivity of graphene is allocated to a single interface whose effective thickness is $t_g = 0.5 \text{nm}$. Based on the above

analysis, the Fermi energy of the graphene rectangular sheets array can be easily modulated by tuning the gate voltage [46]. In the context of the particular phase distribution designing that can induce anomalous reflection on metasurfaces, the dynamic steering of the terahertz beam can be achieved by tuning the dielectric property of graphene. For experimental characterization, the proposed graphene metasurface can be fabricated by following procedures. At first, a monolayer graphene grown on copper by chemical vapor deposition (CVD) method is transferred to the MgF₂ substrate with a gold reflective layer, utilizing the wet chemical transfer process [47–49]. Then, the graphene can be patterned by photolithography and reactive ion etching (RIE) with oxygen plasma. Finally, the top gate electrodes can be fabricated using electron beam evaporation through shadow masks [50,51].

3. Results and discussion

3.1. Tunable response of graphene sheet

Graphene sheets can strongly respond to terahertz electromagnetic waves due to plasmonic excitation at proper Fermi energies [52]. In order to explore the tunable response of graphene sheets, we take a unit cell building block as an example for analysis, as shown in Fig. 2(a). The parameters of the element are chosen as $G_x = G_y = 5.0 \mu\text{m}$, $k = 0.5 \mu\text{m}$, $P_y = 6 \mu\text{m}$, and $P_x + G_x = k$. In our calculation, the frequency of the light is set to be 5.0 THz. The linearly polarized light is normally incident on the graphene sheets, and its polarization is parallel to the x axis. In the above structural model, the metasurface layer and the metallic substrate are acting as partial and full reflectors respectively, which can be considered as an asymmetrical Fabry-Perot resonator.

The amplitude and phase of the reflected light can be continuously adjusted by varying the graphene Fermi energy, as shown in Fig. 2(b). It can be observed that the reflected light phase is fixed at 0° when the Fermi energy is set to 0 eV. The phase can smoothly vary from 0° to 200° with the increase of Fermi energy. Meanwhile, the amplitude transfer coefficient of the reflected light is always maintained at high level (≥ 0.8). Besides, the insets in Fig. 2(b) are the relative magnitude of electric fields at three Fermi energies of 0.1 eV, 0.5 eV and 0.9 eV, respectively. Obviously, it can be inferred from the difference of the intensity field that the optical response of the metasurface can be effectively modulated by the graphene Fermi energy.

To realize the function of beam steering by uniformly adjusting the Fermi energy of graphene, the gradient distribution of phase-changing-rate is necessary to be achieved. However, traditional methods can not satisfy our demand (see Supplement 1, Note S2). In this case, we propose the design scheme of nonuniform periodic structures. In our design, G_x and G_y are adjusted independently. As shown in Fig. 1(b), the adjustment of geometric parameters is divided into two sections: Section I, $P_x = 5.5 \mu\text{m}$, $P_y = 6.0 \mu\text{m}$, $G_x = 5.0 \mu\text{m}$, and the size of graphene in y direction (G_y) increases gradually (from 0 μm to 5.0 μm). Section II, $P_y = 6.0 \mu\text{m}$, $G_y = 5.0 \mu\text{m}$, the size of graphene in x direction (G_x) decreases gradually (from 5.0 μm to 0 μm), and the following relationship is satisfied: $P_x + G_x = k$. Based on the above parameters, Figs. 2(c) and 2(d) show the phase and amplitude of the reflected light with varied device physical dimensions as the function of the graphene Fermi energies. In order to keep the reflection intensity stable, only the region below the dash line is selected as the alternative data set. For clarity, several groups of data are picked out and exhibited in Figs. 2(e) and 2(f). As shown in Fig. 2(c), it demonstrates that the phase-changing-rate is gradually increasing from the bottom to the top, which means that the gradient distribution of phase-changing-rate is realized. Figure 2(e) shows that the maximum phase coverage reaches 300° as the Fermi energy increases from 0 eV to 1.1 eV. It is obtained from Figs. 2(d) and 2(f) that the reflection amplitude is always above 0.6 in the selected region. Based on these properties, we can straightforwardly select unit cells from the data set for the designing of functional devices.

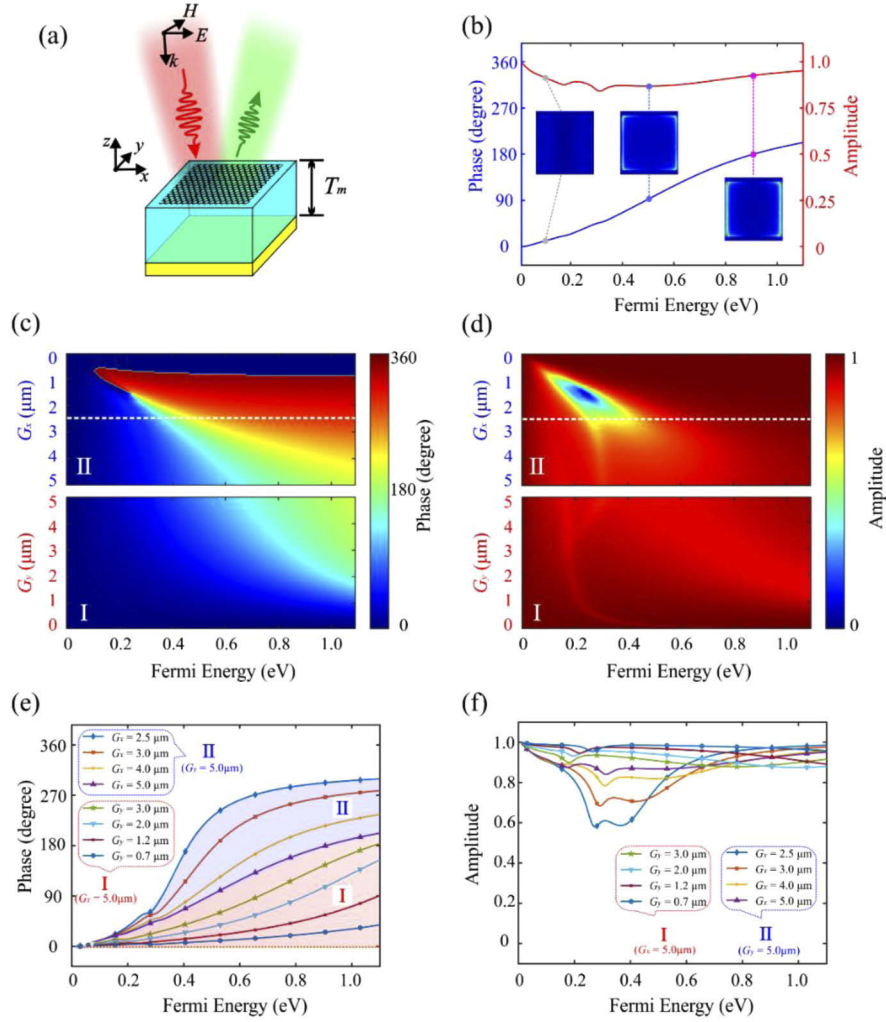


Fig. 2. (a) Schematic of the unit cell containing the graphene sheet, $P_x = 5.5 \mu\text{m}$, $P_y = 6.0 \mu\text{m}$, $G_x = G_y = 5.0 \mu\text{m}$, and $k = 0.5 \mu\text{m}$. (b) Phase and Amplitude of the reflected with varied Fermi energies. The insets show the relative magnitude of electric field at three Fermi energies of 0.1 eV, 0.5 eV and 0.9 eV, respectively. (c), (e) Relative phase and (d), (f) amplitude of the reflection as functions of Fermi energy and the geometric parameters of graphene sheet.

3.2. Continuously tunable beam scanner

As above mentioned, a series of interesting applications based on graphene metasurfaces have been demonstrated to manipulate electromagnetic waves arbitrarily, such as beam steering device and planar focal lens [53,54]. The first functional device designed in our work is a continuously tunable beam scanner, as shown in Fig. 3(a). To steer the reflected light, we utilize the generalized version of Snell's law to calculate the linearly varied phase shift along the device surface [55]:

$$\sin \theta_r - \sin \theta_i = \frac{\lambda}{2\pi n_i} \frac{d\Phi}{dx} \quad (3)$$

where θ_r is representing the reflection angle, θ_i the incident angle, n_i the refractive index of the input media, λ the vacuum wavelength of light, $d\Phi$ and dx respectively represent the phase difference and geometric distance between adjacent units. In contrast with conventional specular reflection, the relation between θ_r and θ_i is nonlinear. Based on the derivation of Eq. (3), the abnormal reflection phenomenon will appear when a constant phase discontinuous gradient ($d\Phi/dx$) is introduced along the interface. When the terahertz beam is incident vertically on the graphene metasurface ($\theta_i = 0^\circ$), the reflected light deviates from the interface normal with a reflection angle: $\theta = \arcsin\left(\frac{\lambda}{2\pi} \frac{d\Phi}{dx}\right)$.

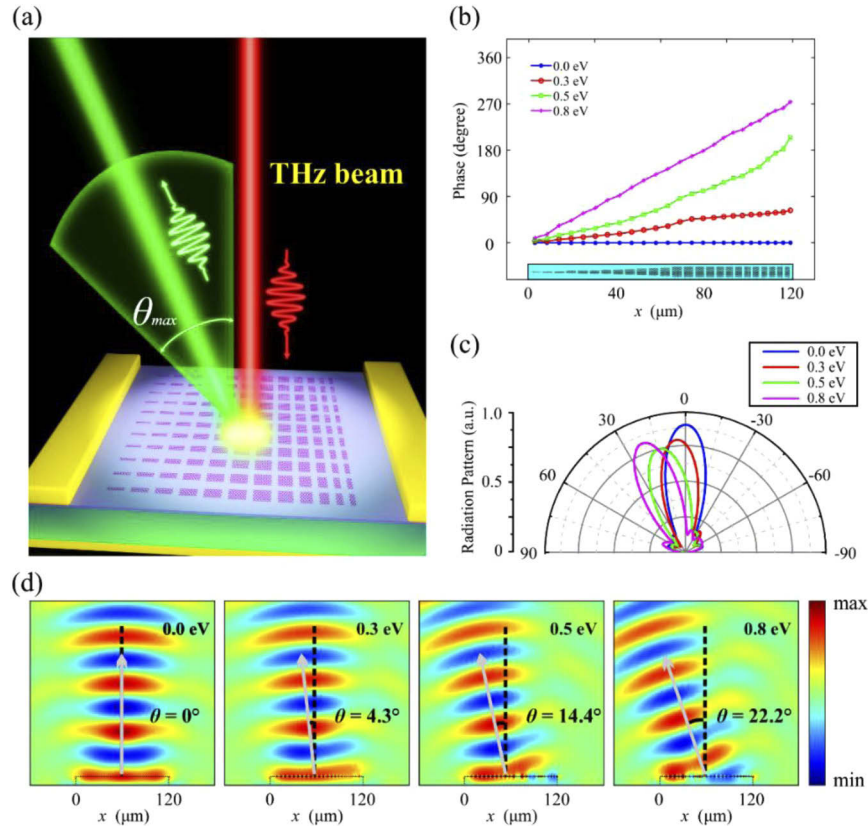


Fig. 3. (a) Schematic representation of the continuously tunable beam scanner, where θ_{max} is the maximum deflection angle. (b) Reflective phase distribution of the super cell at the selected Fermi energies: 0.0 eV, 0.3 eV, 0.5 eV, 0.8 eV. The inset is the schematic of the super cell with the length of $L = 120 \mu\text{m}$. (c) Radiation patterns and (d) electric-field distribution of the reflected waves.

Moreover, to realize the gradient distribution of the phase-changing-rate, we carefully calculated the geometrical dimensions of the rectangular sheets by considering the above optical response analysis above. In our simulation, we choose a group of cells as a super cell, whose length is set as L . Firstly, the length of the super cell L is fixed at about $120 \mu\text{m}$, and the maximum phase range is reached when its Fermi energy is around 0.8 eV. Secondly, the phase distribution should satisfy the formula: $d\Phi(x)/dx = b$, where b is a constant associated with Fermi energy. Figure 3(b) exhibits that the super cell contains 25 units, and the lengths of G_x and G_y of the graphene sheets are list detailedly in Supplement 1 (see Note S3 and Table S1). The size of the element in x direction P_x is the sum of G_x and the gap between graphene sheets k . As the Fermi

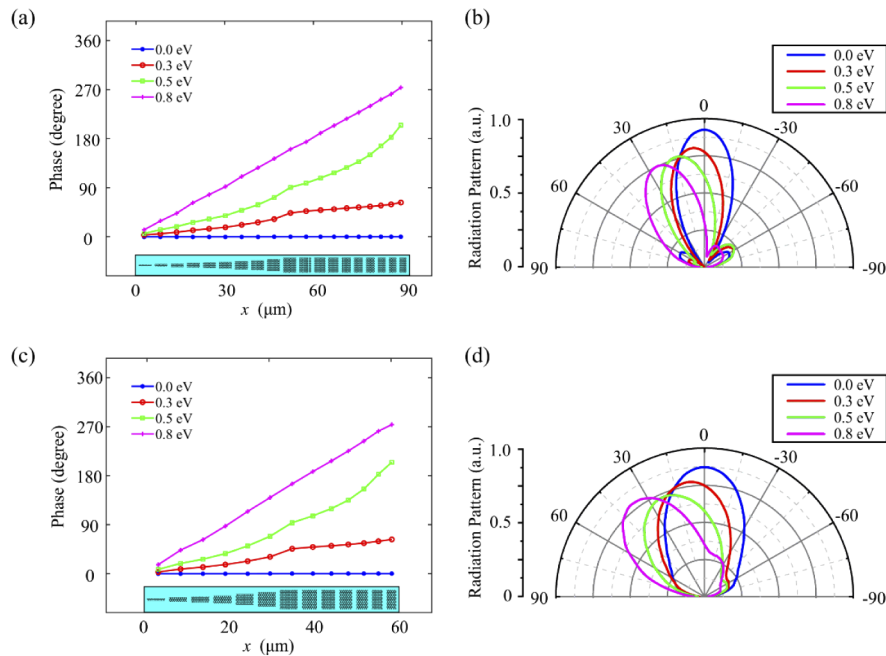


Fig. 4. Reflective phase distribution of the super cell at the selected Fermi energies, when (a) $L = 90 \mu\text{m}$ and (c) $L = 60 \mu\text{m}$. (b) and (d) are corresponding radiation patterns of the reflected waves, respectively.

energy increase from 0.0 eV to 0.8 eV, the phase coverage range increase. Figure 3(b) shows the phase distribution of the super cell corresponding to the Fermi energies of 0.0 eV, 0.3 eV, 0.5 eV and 0.8 eV, respectively. The radiation patterns and corresponding electric-field distribution of the reflected waves are exhibited in Figs. 3(c) and 2(d). It can be seen from these figures that the effective beam scanning by uniformly adjusting the Fermi energy of graphene is achieved. The reflection angle θ increases continuously with the increase of Fermi energy. As the Fermi energy is assumed to be 0.8 eV, the maximum deflection angle (θ_{max}) reaches 22.2° , and the corresponding phase coverage range is 290° . Obviously, the relative radiation intensity of the beam is always above 0.75, when the deflection angle changes.

For further research, two improved beam scanners are proposed to optimize the scanning performance. The lengths of the super cells are fixed at $90 \mu\text{m}$ and $60 \mu\text{m}$. The parameters of unit structural contained in the super cells are listed in Supplement 1 (see Tables S2 and S3). Figure 4 shows the phase distribution and radiation patterns of the optimized scanners at different Fermi energies. It is seen that the coverage range of the phase still reaches 290° at 0.8 eV, while the maximum deflection angle increases with the decrease of L . Figures 4(b) and 4(d) illustrate the scanning function is well maintained. The deflection angle of the scanning beam changes continuously and the radiation intensity remains stable with the adjustment of Fermi energy. The maximum deflection angles of the scanners are 26.4° ($L = 90 \mu\text{m}$) and 35.5° ($L = 60 \mu\text{m}$). From the above analysis, it can be inferred that the scanning range of the scanner is constantly expanding with the decrease of L , while the directivity of the radiation beam is getting worse. One possible reason is that the scattering effect affects the quality of the radiation beams.

In the above research, the working frequency of the beam scanner we designed was limited to $f_0 = 5.0 \text{ THz}$. While, the scanning capability of the beam scanner is effective in a broadband range. Here, we studied the broadband performance of these scanners ($L = 120 \mu\text{m}$, $90 \mu\text{m}$ and $60 \mu\text{m}$). The deflection angle reaches maximum at the Fermi energy of 0.8 eV. Figure 5 illustrates

the maximum deflection angle of scanners in the frequency range from 4.0 to 6.4 THz. As shown in Figs. 5(a) and 5(b), the maximum deflection angle increases with the decrease of frequency, which is consistent with calculation of Eq. (3). However, the situation in Fig. 5(c) is different, where the maximum deflection angle decreases with the decrease of frequency. There are two main reasons that cause this phenomenon. First, the phase modulation ability of the graphene unit is weakened with the changing of frequency. Second, the ratio of wavelength and the length of super cell decreases with the decrease of frequency, which leads to the enhancement of the scattering effect. The scattering effect is directionless which causes serious disturbance to the directivity of the radiation beam. Therefore, the balance between scanning range and directivity should be considered in practice.

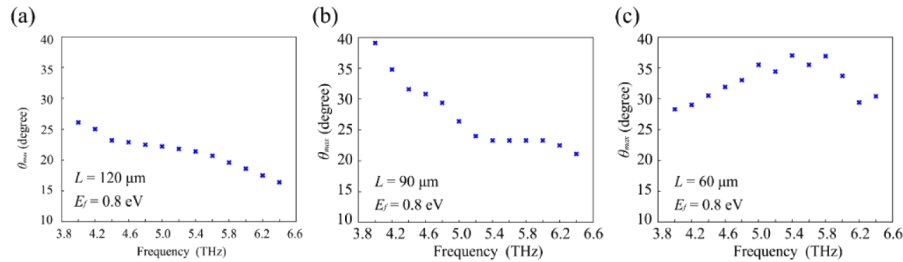


Fig. 5. The maximum deflection angle ($E_f = 0.8$ eV) of scanners with lengths of (a) 120 μm , (b) 90 μm and (c) 60 μm at different incident frequency.

3.3. Variable-focus reflective metalens

The second metasurface we proposed and demonstrated is a uni-electrode-controlled variable-focus reflective metalens, as shown in Fig. 6(a). To design such a metalens whose center is at the origin of x -axis, the phase shift distribution $\varphi(x)$ should satisfy the following equation [30]:

$$\varphi(x) = \frac{2\pi}{\lambda} \left(\sqrt{F^2 + x^2} - F \right) \quad (4)$$

where x and F are representing the position of graphene unit the designed focal length, respectively. According to the phase response characteristic shown in Fig. 2, when the parameters of the cells are fixed, the phase-changing-rate of the side structures is faster than that of the center. Therefore, the phase curve and the focal length can be adjusted dynamically and continuously by varying the graphene Fermi energy.

In our calculation, several parameters are predetermined: the designed focal length $F_0 = 600$ μm , Fermi energy $E_f = 0.5$ eV, and the frequency $f = 5.0$ THz. Figure 6(b) shows the theoretical phase distribution of the metalens. In order to match the phase distribution derived by Eq. (4), the geometrical parameters of graphene sheets can be selected from the data set presented in Fig. 2 (see Supplement 1, Table S4). The linearly polarized incident light (E_x) vertically irradiates on the graphene metasurface. It can be indicated from Fig. 6(c) that the focusing effect of the reflected wave is quite obvious. The actual calculated focal length is $F = 530$ μm , which is consistent with the original design. As shown in Fig. 6(b), the simulation result of the phase distribution is approximately consistent with the theoretical analysis. There exists reasonable difference between the design and simulation results, for the reason that the finite size of device introduces the scattering influence.

We validate the tunability of the variable-focus reflective metalens by simulating the focusing effect at different Fermi energies (from 0.4 to 0.9 eV). As exhibited in Fig. 7(a), the phase distribution of the metalens changes significantly with the varying of Fermi energy, which is consistent with the expected inference. In Fig. 7(b), the focal length increases from 385 μm to

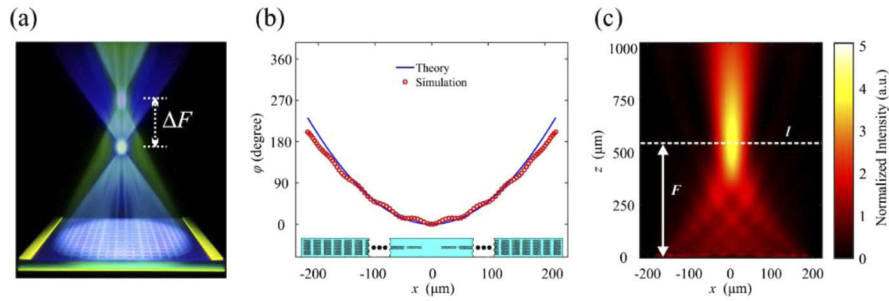


Fig. 6. (a) Schematic representation of the variable-focus reflective metalens, where ΔF is the adjustable range of the focal spot. (b) Theoretical and simulated phase distribution of the metalens at the frequency of $f_0 = 5.0$ THz, in which the designed focal length is $F = 600$ μm and the Fermi energy is fixed at $E_f = 0.5$ eV. (c) Intensity field distribution of the reflected light on the x - z plane. The simulated focal length is 530 μm .

666 μm as Fermi energy decreases from 0.9 to 0.4 eV, with a focal shift of about 281 μm . The corresponding intensity field distribution is exhibited in Fig. 7(c), indicating that the focusing effect is well maintained in the process of dynamic adjustment.

In addition, the focusing characteristics and adjustable performance of the designed device are effective in broadband range. Figure 8 illustrates the broadband performance of focusing modulation in a frequency range of from 3.6 to 5.6 THz. It is obvious that the adjustable range of the focal length is maximized at the frequency of 5.0 THz. The frequency deviation from the initial frequency will lead to the decrease of the modulation range. It can be indicated from

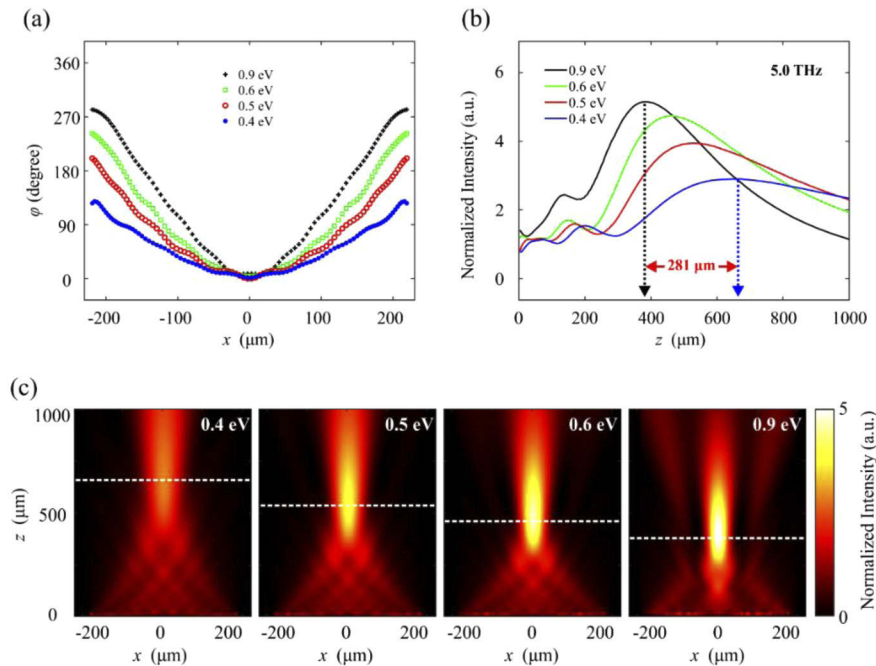


Fig. 7. (a) Phase distribution of the metalens at frequency $f_0 = 5.0$ THz, when the Fermi energy increases from 0.4 eV to 0.9 eV. Corresponding (b) intensity field distribution of the reflected light along the z -axis and (c) focusing effect of the metalens.

the Fig. 8 that the focal length decreases with the decrease of the incident frequency. To our knowledge, the axial chromatic aberration can be adopted to explain the phenomenon above. [56]. So far, the proposed variable-focus reflective metalens modulated by uniform bias-voltage has been proved to be practical.

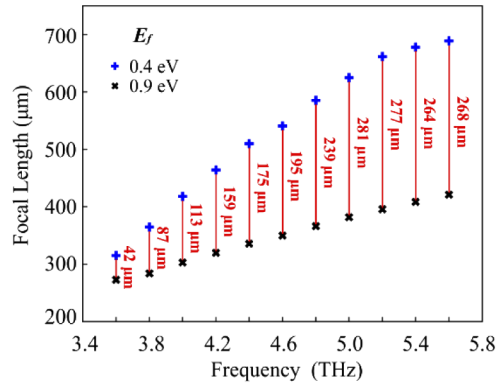


Fig. 8. Tuning range of the focal length at different frequencies, when the Fermi energy increased from 0.4 eV to 0.9 eV.

4. Conclusion

In conclusion, we have demonstrated a series of metasurfaces based on nonuniform periodic graphene structures, whose optical response can be continuously modulated by uniform bias-voltage. The optical responses of nonuniform periodic graphene sheets was studied systematically. By carefully tailoring the geometrical parameters of the rectangular sheets, the gradient distribution of the reflected light phase-changing-rate was realized. A beam scanner and a variable-focus reflective metalens were demonstrated with a working frequency of 5.0 THz, which is enabled by uniformly adjusting the graphene Fermi energy. Moreover, with the excellent scalability of metasurfaces, the scanning function of the scanner and the dynamic focusing function of the metalens were preserved in a broadband frequency range. The graphene metasurfaces with ultrathin thickness proposed in our work provided a potential way to miniaturize the optical systems for terahertz communication, holographic imaging and other wavefront controlling devices.

Funding

National Natural Science Foundation of China (60907003, 61805278); Natural Science Foundation of Hunan Province (13JJ300); Program for New Century Excellent Talents in University (NCET-12-0142); China Postdoctoral Science Foundation (2018M633704); Foundation of NUDT ((JC13-02-13, ZK17-03-01); Hunan Provincial Innovation Foundation for Postgraduate (CX20200039).

Disclosures

No conflict of interest exists in the submission of this manuscript.

See [Supplement 1](#) for supporting content

References

1. R. A. Shelby, D. R. Smith, and S. Schultz, "Experimental verification of a negative index of refraction," *Science* **292**(5514), 77–79 (2001).
2. A. V. Kildishev, A. Boltasseva, and V. M. Shalaev, "Planar Photonics with Metasurfaces," *Science* **339**(6125), 1232009 (2013).
3. N. Yu and F. Capasso, "Flat optics with designer metasurfaces," *Nat. Mater.* **13**(2), 139–150 (2014).
4. C. L. Holloway, E. F. Kuester, J. A. Gordon, J. F. O'Hara, J. Booth, and D. R. Smith, "An Overview of the Theory and Applications of Metasurfaces: The Two-Dimensional Equivalents of Metamaterials," *IEEE Antennas Propag. Mag.* **54**(2), 10–35 (2012).
5. X. Luo, "Principles of electromagnetic waves in metasurfaces," *Sci. China: Phys., Mech. Astron.* **58**(9), 594201 (2015).
6. N. Yu, P. Genevet, M. A. Kats, F. Aieta, J. Tetienne, F. Capasso, and Z. Gaburro, "Light Propagation with Phase Discontinuities: Generalized Laws of Reflection and Refraction," *Science* **334**(6054), 333–337 (2011).
7. Y. Liu and X. Zhang, "Metamaterials: a new frontier of science and technology," *Chem. Soc. Rev.* **40**(5), 2494–2507 (2011).
8. C. M. Costas and M. Wegener, "Past achievements and future challenges in the development of three-dimensional photonic metamaterials," *Nat. Photonics* **5**(9), 523–530 (2011).
9. D. R. Smith, J. B. Pendry, and M. C. K. Wiltshire, "Metamaterials and Negative Refractive Index," *Science* **305**(5685), 788–792 (2004).
10. Y. J. Tsai, S. Larouche, T. Tyler, G. Lipworth, N. M. Jokerst, and D. R. Smith, "Design and fabrication of a metamaterial gradient index diffraction grating at infrared wavelengths," *Opt. Express* **19**(24), 24411–24423 (2011).
11. A. Nemati, Q. Wang, M. Hong, and J. Teng, "Tunable and reconfigurable metasurfaces and metadevices," *Opto-Electron. Adv.* **1**(5), 18000901–18000925 (2018).
12. C. Pfeiffer, N. K. Emani, A. M. Shaltout, A. Boltasseva, V. M. Shalaev, and A. Grbic, "Efficient Light Bending with Isotropic Metamaterial Huygens' Surfaces," *Nano Lett.* **14**(5), 2491–2497 (2014).
13. J. Neu, R. Beigang, and M. Rahm, "Metamaterial-based gradient index beam steerers for terahertz radiation," *Appl. Phys. Lett.* **103**(4), 041109 (2013).
14. J. Lin, J. P. B. Mueller, Q. Wang, G. Yuan, N. Antoniou, X. Yuan, and F. Capasso, "Polarization-Controlled Tunable Directional Coupling of Surface Plasmon Polaritons," *Science* **340**(6130), 331–334 (2013).
15. N. Yu, F. Aieta, P. Genevet, M. A. Kats, Z. Gaburro, and F. Capasso, "A Broadband, Background-Free Quarter-Wave Plate Based on Plasmonic Metasurfaces," *Nano Lett.* **12**(12), 6328–6333 (2012).
16. Z. Wei, Y. Ca, X. Su, Z. Gong, Y. Long, and H. Li, "Highly efficient beam steering with a transparent metasurface," *Opt. Express* **21**(9), 10739–10745 (2013).
17. G. Zheng, H. Mühlenbernd, M. Kenney, G. Li, T. Zentgraf, and S. Zhang, "Metasurface holograms reaching 80% efficiency," *Nat. Nanotechnol.* **10**(4), 308–312 (2015).
18. P. Moitra, B. A. Slovick, Z. Yu, S. Krishnamurthy, and J. Valentine, "Experimental demonstration of a broadband all-dielectric metamaterial perfect reflector," *Appl. Phys. Lett.* **104**(17), 171102 (2014).
19. F. Capasso, F. Aieta, M. Khorasaninejad, P. Genevet, and R. Devlin, "Recent advances in planar optics: from plasmonic to dielectric metasurfaces," *Optica* **4**(1), 139 (2017).
20. D. Lin, P. Fan, E. Hasman, and M. L. Brongersma, "Dielectric gradient metasurface optical elements," *Science* **345**(6194), 298–302 (2014).
21. Y. Gu, X. Ma, M. Pu, X. Li, Z. Zhao, and X. Luo, "High-Efficiency and Wide-Angle Beam Steering Based on Catenary Optical Fields in Ultrathin Metalens," *Adv. Opt. Mater.* **6**(19), 1800592 (2018).
22. V. Yachin, L. Ivzhenko, S. Polevoy, and S. Tarapov, "Resonant response in mechanically tunable metasurface based on crossed metallic gratings with controllable crossing angle," *Appl. Phys. Lett.* **109**(22), 221905 (2016).
23. H. Ee and R. Agarwal, "Tunable Metasurface and Flat Optical Zoom Lens on a Stretchable Substrate," *Nano Lett.* **16**(4), 2818–2823 (2016).
24. Z. Wang, L. Jing, K. Yao, Y. Yang, B. Zheng, C. M. Soukoulis, H. Chen, and Y. Liu, "Origami-Based Reconfigurable Metamaterials for Tunable Chirality," *Adv. Mater.* **29**(27), 1700412 (2017).
25. C. Luo, D. Li, J. Yao, and F. Ling, "Direct thermal tuning of the terahertz plasmonic response of semiconductor metasurface," *J. Electromagn. Waves Appl.* **29**(18), 2512–2522 (2015).
26. S. Khatua, W. Chang, P. Swanglap, J. Olson, and S. Link, "Active Modulation of Nanorod Plasmons," *Nano Lett.* **11**(9), 3797–3802 (2011).
27. A. K. Geim and K. S. Novoselov, "The rise of graphene," *Nat. Mater.* **6**(3), 183–191 (2007).
28. F. H. L. Koppens, D. E. Chang, and G. F. J. de Abajo, "Graphene plasmonics: a platform for strong light-matter interactions," *Nano Lett.* **11**(8), 3370–3377 (2011).
29. Z. Li, K. Yao, F. Xia, S. Shen, J. Tian, and Y. Liu, "Graphene Plasmonic Metasurfaces to Steer Infrared Light," *Sci. Rep.* **5**(1), 12423 (2015).
30. W. Ma, Z. Huang, X. Bai, P. Zhan, and Y. Liu, "Dual-Band Light Focusing Using Stacked Graphene Metasurfaces," *ACS Photonics* **4**(7), 1770–1775 (2017).
31. S. Thongrattanasiri, F. H. L. Koppens, and G. F. J. de Abajo, "Complete optical absorption in periodically patterned graphene," *Phys. Rev. Lett.* **108**(4), 047401 (2012).

32. Z. Zeng, X. Huang, Z. Yin, H. Li, Y. Chen, H. Li, Q. Zhang, J. Ma, F. Boey, and H. Zhang, "Fabrication of Graphene Nanomesh by Using an Anodic Aluminum Oxide Membrane as a Template," *Adv. Mater.* **24**(30), 4138–4142 (2012).
33. Z. Zhang, X. Yan, L. Liang, D. Wei, M. Wang, Y. Wang, and J. Yao, "The novel hybrid metal-graphene metasurfaces for broadband focusing and beam-steering in farfield at the terahertz frequencies," *Carbon* **132**, 529–538 (2018).
34. Z. Su, X. Chen, J. Yin, and X. Zhao, "Graphene-based terahertz metasurface with tunable spectrum splitting," *Opt. Lett.* **41**(16), 3799–3802 (2016).
35. Z. Fang, S. Thongrattanasiri, A. Schlather, L. Zheng, L. Ma, Y. Wang, P. M. Ajayan, P. Nordlander, N. J. Halas, and G. F. J. de Abajo, "Gated Tunability and Hybridization of Localized Plasmons in Nanostructured Graphene," *ACS Nano* **7**(3), 2388–2395 (2013).
36. A. Fallahi and J. Perruisseau-Carrier, "Design of tunable biperiodic graphene metasurfaces," *Phys. Rev. B* **86**(19), 195408 (2012).
37. Z. Su, F. Cheng, L. Li, and Y. Liu, "Complete Control of Smith-Purcell Radiation by Graphene Metasurfaces," *ACS Photonics* **6**(8), 1947–1954 (2019).
38. A. Vakil and N. Engheta, "Transformation Optics Using Graphene," *Science* **332**(6035), 1291–1294 (2011).
39. P. Chen, M. Farhat, A. N. Askarpour, M. Tymchenko, and A. Alù, "Infrared beam-steering using acoustically modulated surface plasmons over a graphene monolayer," *J. Opt.* **16**(9), 094008 (2014).
40. C. Shi, I. J. Luxmoore, and G. R. Nash, "Gate tunable graphene-integrated metasurface modulator for mid-infrared beam steering," *Opt. Express* **27**(10), 14577–14584 (2019).
41. T. Yatooshi, A. Ishikawa, and K. Tsuruta, "Terahertz wavefront control by tunable metasurface made of graphene ribbons," *Appl. Phys. Lett.* **107**(5), 053105 (2015).
42. H. Xu, W. Lu, Y. Jiang, and Z. Dong, "Beam-scanning planar lens based on graphene," *Appl. Phys. Lett.* **100**(5), 051903 (2012).
43. P. Ding, Y. Li, L. Shao, X. Tian, J. Wang, and C. Fan, "Graphene aperture-based metalens for dynamic focusing of terahertz waves," *Opt. Express* **26**(21), 28038–28050 (2018).
44. V. Thareja, J. Kang, H. Yuan, K. M. Milaninia, H. Y. Hwang, Y. Cui, P. G. Kik, and M. L. Brongersma, "Electrically Tunable Coherent Optical Absorption in Graphene with Ion Gel," *Nano Lett.* **15**(3), 1570–1576 (2015).
45. L. A. Falkovsky, "Optical properties of graphene," *J. Phys.: Conf. Ser.* **129**(1), 012004 (2008).
46. K. S. Novoselov, A. K. Geim, S. V. Morozov, D. Jiang, M. I. Katsnelson, I. V. Grigorieva, S. V. Dubonos, and A. A. Firsov, "Two-Dimensional Gas of Massless Dirac Fermions in Graphene," *Nature* **438**(7065), 197–200 (2005).
47. C. Wang, W. Liu, Z. Li, H. Cheng, Z. Li, S. Chen, and J. Tian, "Dynamically Tunable Deep Subwavelength High-Order Anomalous Reflection Using Graphene Metasurfaces," *Adv. Opt. Mater.* **6**(3), 1701047 (2018).
48. B. J. Kim, H. Jang, S. K. Lee, B. H. Hong, J. Ahn, and J. H. Cho, "High-Performance Flexible Graphene Field Effect Transistors with Ion Gel Gate Dielectrics," *Nano Lett.* **10**(9), 3464–3466 (2010).
49. G. Deokar, J. Avila, I. Rizado-colambo, J. L. Codron, C. Boyaval, E. Galopin, M. C. Asensio, and D. Vignaud, "Towards high quality CVD graphene growth and transfer," *Carbon* **89**, 82–92 (2015).
50. Y. Zhang, Y. Feng, T. Jiang, J. Cao, J. Zhao, and B. Zhu, "Tunable broadband polarization rotator in terahertz frequency based on graphene metamaterial," *Carbon* **133**, 170–175 (2018).
51. Q. Li, Z. Tian, X. Zhang, R. Singh, L. Du, J. Gu, J. Han, and W. Zhang, "Active graphene–silicon hybrid diode for terahertz waves," *Nat. Commun.* **6**(1), 7082 (2015).
52. J. Christensen, A. Manjavacas, S. Thongrattanasiri, F. H. L. Koppens, and G. F. J. de Abajo, "Graphene plasmon waveguiding and hybridization in individual and paired nanoribbons," *ACS Nano* **6**(1), 431–440 (2012).
53. L. Deng, Y. Wu, C. Zhang, W. Hong, B. Peng, J. Zhu, and S. Li, "Manipulating of Different-Polarized Reflected Waves with Graphene-based Plasmonic Metasurfaces in Terahertz Regime," *Sci. Rep.* **7**(1), 10558 (2017).
54. X. Zhang, Z. Tian, W. Yue, J. Gu, S. Zhang, J. Han, and W. Zhang, "Broadband Terahertz Wave Deflection Based on C-shape Complex Metamaterials with Phase Discontinuities," *Adv. Mater.* **25**(33), 4567–4572 (2013).
55. H. Cheng, S. Chen, P. Yu, W. Liu, Z. Li, J. Li, B. Xie, and J. Tian, "Dynamically Tunable Broadband Infrared Anomalous Refraction Based on Graphene Metasurfaces," *Adv. Opt. Mater.* **3**(12), 1744–1749 (2015).
56. D. Tang, C. Wang, Z. Zhao, Y. Wang, M. Pu, X. Li, P. Gao, and X. Luo, "Ultrabroadband superoscillatory lens composed by plasmonic metasurfaces for subdiffraction light focusing," *Laser Photonics Rev.* **9**(6), 713–719 (2015).